PERGAMON

International Journal of Heat and Mass Transfer 44 (2001) 2299–2310

International Journal of HEAT and MASS TRANSFER

www.elsevier.com/locate/ijhmt

Experimental investigation on ammonia spray evaporator with triangular-pitch plain-tube bundle, Part I: tube bundle effect

X. Zeng [a,1], M.-C. Chyu [a,*], Z.H. Ayub [b]

[a] *Department of Mechanical Engineering, Texas Tech University, Mail Stop 1021, P.O. Box 41021, Lubbock, TX 79409-1021, USA*
[b] *Isotherm, Inc., Arlington, TX 76003-0206, USA*

Received 24 August 1999; received in revised form 14 July 2000

Abstract

The experiment of spray evaporation of ammonia was conducted using spray nozzles distributing liquid ammonia downward onto a horizontal, 3–2–3 triangular-pitch plain-tube bundle. Heat transfer performance of individual tubes in the tube bundle was studied by changing saturation temperature, heat flux, spray flow rate, nozzle height, and nozzle type. The present data suggest that the tube bundle effect is less significant at a lower saturation temperature, a lower spray flow rate, a smaller nozzle height, and with standard-angle compared with wide-angle nozzles. Mechanism causing variation of individual tubes' heat transfer performance was studied. Results were compared with ammonia spray evaporation in a square-pitch plain-tube bundle.

1. Introduction

Alternative refrigerants suitable for refrigeration systems have been actively investigated owing to increasingly more regulations placed on the use of chlorofluorocarbon-based (CFC) refrigerants, as well as the scheduled phaseout of CFCs and hydrofluorocarbons (HCFCs) altogether. Ammonia has been considered as an important alternative refrigerant for new and existing large centralized refrigerating, air-conditioning systems, and thermal storage systems. Ammonia has a 0.00 value of ozone depletion potential (ODP) when released to atmosphere, and does not directly contribute to global warming. It also has a low boiling point and high latent heat of vaporization (about 9 times greater than R-12 or R-22). These characteristics make ammonia a highly energy-efficient refrigerant with minimal potential environmental problems [1].

Based on safety concerns, it is desirable to reduce the amount of ammonia as the refrigerant required to charge the system. By employing a spray evaporator in the refrigeration system, the required amount of ammonia may be greatly reduced compared with flooded evaporator, and the system performance may be significantly enhanced [2]. In a horizontal-tube spray evaporator, liquid is sprayed downward onto the top of a horizontal tube bundle and flowing on the tubes' outside walls while being evaporated. The liquid run-off is re-circulated along with the return from the condenser. In addition to a reduced liquid inventory requirement, advantages of horizontal-tube spray evaporator include high heat transfer performance, lower leakage hazard potential, no hydrostatic head effect, convenience in operation, etc. Spray evaporators were tested with new, ozone-friendly, but more costly refrigerants such as R-123 and R-134a for the purpose of reducing the refrigerant inventory in order to achieve cost saving [3–8].

Spray evaporation has been widely studied in terms of effects such as liquid feed flow rate, liquid distribution method, liquid feed flow pattern, liquid feed temperature, tube spacing, heat flux, tube surface structure, surface aging, surface subcooling, vapor cross-flow, etc. A comprehensive literature reviews of spray film evaporation on plain and enhanced single tubes and tube bundles was presented recently by Thome [9]. Literature survey on spray evaporation on a single horizontal plain

* Corresponding author. Tel.: +1-806-742-3563; fax: +1-806-742-3540.
E-mail address: mchyu@coe.ttu.edu (M.-C. Chyu).
[1] Present address: General Motors Corporation, Warren, MI 48090-9025, USA.

0017-9310/01/$ - see front matter
PII: S0017-9310(00)00250-7

Nomenclature

A	heat transfer area
a	length of overlap spray region between nozzles
D	tube diameter
d	nozzle height, viz distance between the nozzle outlet and the top of the horizontal tube bundle
h	heat transfer coefficient
i	enthalpy
k	thermal conductivity
L	distance between the two adjacent nozzles
$\dot{m}$	spray mass flow rate
$\dot{m}_t$	tube-side mass flow rate
q	heat transfer rate
q''	heat flux
r	tube radius
T	temperature
ΔT_{lm}	log-mean temperature difference
U	overall heat transfer coefficient
$\dot{V}$	volumetric flow rate

Greek symbol

Γ_l	average mass flow rate of sprayed liquid reaching a tube bundle per unit tube length

Subscripts

i	inside
l	liquid
n	per nozzle
o	outside, shell side
s	saturation
t	tube

tube was also conducted by Zeng et al. [10], and that on a horizontal plain-tube bundle by Zeng et al. [11], including early works on spray evaporation of sea water for desalination [12–16], and those on spray evaporation of ammonia on a triangular-pitch bundle of tubes with porous coating for Ocean Thermal Energy Conversion (OTEC) System [17–20]. With regard to application in refrigeration, Danilova et al. [21] conducted spray evaporation of CFC and HCFC refrigerants in a plain tube bundle. A series of spray evaporation tests were recently performed by Moeykens, Pate and co-authors by including R-134a on single horizontal plain tube [3], seven different single-enhanced tubes [6], square- and triangular-pitch enhanced tube bundles [4,7]. Tests were also reported with R-22 in triangular-pitch tube bundles made from enhanced-condensation, enhanced-boiling, low-finned, and plain-surface tubes [8], and with R-123 on triangular-pitch tube bundles of enhanced-condensation, enhanced-boiling, and plain-surface tubes [5].

Based on the consideration of corrosion hazard, steel is the most common material used in ammonia systems. A problem associated with ammonia spray evaporation is ammonia's poor wetting capability on steel surfaces despite ammonia's low surface tension. It has been reported that liquid ammonia distributed by a low-momentum perforated tube distributor formed a small number of rivulets making irregular paths over the curved tube surfaces [22]. To overcome this problem, spray nozzles generating high-momentum liquid spray that could improve both the heat transfer and the surface wetting condition were employed recently in few studies. High-momentum commercial spray nozzles were employed in the spray evaporation experiments of ammonia by Zeng et al. [10] for single plain tube, for single low-fin and corrugated tubes [23], and for square-pitch plain-tube bundle [11]. Spray nozzles were also used in spray evaporation tests with fluids other than ammonia [3–8,20,24,25]. A study of spray flow distribution in a square-pitch bundle and a triangular-pitch bundle of plain and low-fin tubes under adiabatic condition was presented by Zeng et al. [26].

For spray evaporation on a tube bundle using nozzles, high heat transfer coefficients are anticipated for tubes in the top row due to the impingement effect of the high-momentum liquid droplets generated by the nozzles. In the lower rows of the tube bundle, the high-momentum spray flow dominates the single-phase convective heat transfer and, in the meantime, plays a role in nucleate boiling as well as the two-phase flow convection featuring turbulence induced by bubbles impinging and sliding over the tube walls, and the consequent thin film evaporation on tube walls. This may result in a significant tube bundle effect featuring variation in the heat transfer coefficients of individual tubes across the bundle, an undesired situation from the heat exchanger operation's point of view. It is the objective of the present work to study the tube bundle effect of a bundle subjected to spray evaporation using spray nozzles, and the effect of a number of parameters on the variation of individual tube coefficients throughout the bundle, including saturation temperature, spray flow rate, nozzle height, and nozzle type. Based on the limitation of the test facility's capacity as well as other factors, a small 3–2–3 triangular-pitch tube bundle was employed which was different from those large bundles tested, for example, for OTEC projects [17–20].

2. Experiment

The experimental facility employed in this study was similar to that of Zeng et al. [10,11,23] for ammonia

spray evaporation. The facility featured a vapor-compression refrigeration cycle including an ammonia spray evaporator, a compressor, a condenser, an expansion device, in addition to an accumulator and a pump, as shown in Fig. 1. The spray evaporator was a cylindrical stainless steel vessel, 61 cm in length and 25.4 cm in diameter, containing seven equally spaced spray nozzles with an 8.9-cm longitudinal interval, as shown in Fig. 2. Also contained in the spray evaporator was a 3–2–3 triangular-pitch tube bundle with all eight tubes in the bundle of commercial stainless steel, and of 19.1 mm (0.75 in.) outside diameter and 15.6 mm (0.61 in.) inside diameter. The tube bundle-pitch ratio was 1.25, a typical value for evaporators used in refrigeration systems. All eight tubes were heated during the experiment by water/ethylene glycol as the heating fluid flowing inside the tube, while ammonia distributed through the nozzles located above the tube bundle was evaporated outside the tubes. The uniformity of the liquid spray flow rate was checked by measuring the quantity of sprayed liquid ammonia collected during a certain period of time at different locations within the area of spray coverage [27]. Seven nozzles were required based on the total ammonia flow rate to the evaporator and the flow rate capacity of each nozzle under the pressure drop corresponding to the test condition. The distance between the nozzles and the top of the tube bundle was adjustable from 0 to 15 cm. The nozzle spray system was designed following the method proposed by Zeng et al. [26]. Both the kinetic energy of the inlet stream and the friction loss in the manifold pipe were very small compared to the pressure drop across the nozzles, so that the flow rate was uniform through all the nozzles [28]. The evaporator vessel was designed for a pressure of 1034 kPa. There was a 17.5-cm diameter Pyrex sight glass window at the center of the evaporator. An O-ring gasket was installed between the tubes and the header sheet at each end of the tubes to seal the shell-side ammonia.

The vapor flow from the evaporator was first conducted to the accumulator where the entrained spray liquid droplets, if any, settled in the bottom, while the dry vapor was directed from the top of the accumulator to the compressor and then to the condenser. The water/ethylene glycol mixture that provided the heat load to

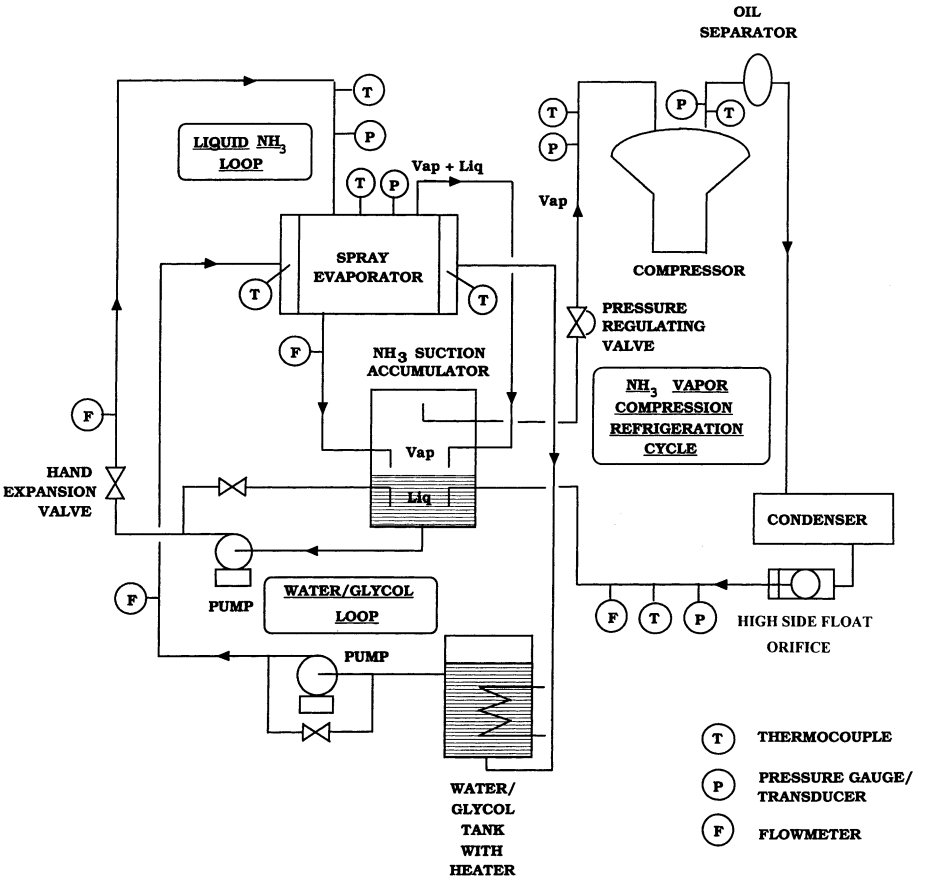

Fig. 1. Experimental facility.

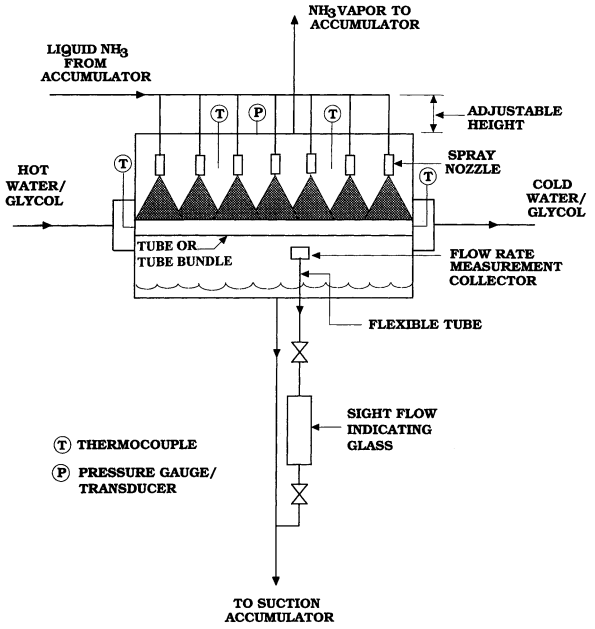

Fig. 2. Experimental spray evaporator.

the evaporator tube bundle was heated in a tank by an electric heater before entering the evaporator. The total heating power to the evaporator was determined by the flow rate indicated by a flowmeter and the change of water/glycol temperature monitored by E-type thermocouples installed at the inlet and the exit of each of the eight evaporator tubes. The saturation temperature of the evaporator was controlled by a pressure regulating valve located at the top of the accumulator. The liquid ammonia run-off collected at the bottom of the spray evaporator was conducted to the accumulator, where it combined with the liquid from the condenser before being circulated back to the evaporator.

Tests were conducted with both standard- and wide-angle commercial nozzles featuring solid cone-shaped spray pattern with a round impact area. The standard-angle nozzles had an orifice diameter of 4.76 mm (3/16 in.) and a spray angle of approximately 90°, while the wide-angle nozzles had an orifice diameter of 3.99 mm (5/32 in.) and a spray angle of approximately 110° under the present test pressure. In order to ensure that the entire tube bundle was well wetted by the liquid spray, the nozzles had to be so arranged that the overlapped impact areas existed between the refrigerant plumes at the top of the tube bundle, and only a fraction of the total nozzle flow rate reached the tube bundle and participated in the evaporation heat transfer process. All the spray evaporation heat transfer data should be characterized by, instead of the total refrigerant flow rate entering the evaporator, the spray flow rate that actually reached the tube bundle. This latter flow rate was measured using a collector and a stopwatch, as described by Chyu et al. [27], for both the standard-angle nozzles and the wide-angle nozzles employed in the present experiment.

During the experiment, the following data were taken: the saturation temperature, the inlet and the exit temperatures and the flow rate of the tube-side flow. The shell-side heat transfer coefficient was determined first using the Wilson plot method [29] as that employed by Zeng et al. [10,11,23] for single tube and tube bundle spray evaporation, as well as numerous other heat transfer research works. The shell-side heat transfer coefficient was determined by extrapolating a plot of $1/U_o$ versus $1/\dot{V}^{0.8}$. The value of $1/h_o + (r_o/k_t)\ \ln(r_o/r_i)$ is given by the intercept of the fitted line with the $1/U_o$-axis, an obvious result from the following equation for the overall heat transfer coefficient with negligible thermal resistance for fouling factors, with $1/h_i = 0$:

$$\frac{1}{U_o} = \frac{r_o}{r_i}\frac{1}{h_i} + \frac{1}{h_o} + \frac{r_o}{k_t}\ln\left(\frac{r_o}{r_i}\right). \tag{1}$$

U_o could be experimentally determined by

$$U_o = \frac{q}{A_o \Delta T_{lm}}, \tag{2}$$

where ΔT_{lm} is the log-mean temperature difference of the evaporator tube, and the heat transfer rate of the tube is calculated by

$$q = \dot{m}_t \Delta i, \tag{3}$$

with Δi being the enthalpy change determined by the decrease of temperature from the inlet to the exit of the

tube. Based on h_o and U_o, h_i was calculated, and was found to compare favorably with the heat transfer coefficient correlation for turbulent tube flow by Gnielinski [30]. The shell-side coefficient h_o was then readily determined by the measured overall coefficient U_o and the calculated tube-side coefficient h_i.

Based on an error analysis, the uncertainty associated with the present shell-side heat transfer coefficient data was estimated to be ±13%, with temperature being the major error source. The error of heat flux was ±4%, and that of local spray flow rate was ±13%. More than half of the tests were repeated, and the repeatability was within 5%.

3. Results and discussion

Ammonia spray evaporation tests ranging from −23°C to 10°C were conducted. In each test, the spray evaporation heat transfer coefficient data for only five tubes were collected which were sufficient to represent the present 3–2–3 tube bundle, due to symmetry. During the experiment, it was observed that similar to square-pitch bundle in spray evaporation [11], most of the interstices between tubes were filled with liquid and vapor mixture moving downward, and there were no clearly defined liquid films flowing on individual tube walls. The entire bundle was hence treated as an evaporator entity, and the spray flow rate per unit length Γ_l participating in the heat transfer within the bundle was determined by the method of Chyu et al. [27] for liquid delivered by an array of nozzles, with D being the width of the bundle. In this method, the local spray flow rate reaching the tube bundle is determined analytically based on a given total nozzle flow rate, nozzle height, nozzle interval, spray angle, tube bundle width, and the horizontal distance between the bundle and the nozzles.

It is noted that the heat transfer coefficient data of tubes in the top row are in all cases the highest among all tubes, due to the effect of liquid droplet impingement. Heat transfer coefficient mostly decreases from the top row towards the bottom row. However, the effect is not as clear at a low temperature, for instance, −23.3°C. A decrease in heat transfer coefficient from the top row to the bottom row was also observed in a five-row spray evaporator of saline water [14,15], and a 3 × 3 square-pitch spray evaporator of ammonia [11]. The present data suggest that the tube bundle effect is less significant at a lower saturation temperature, a lower spray flow rate, a smaller nozzle height, and with standard-angle rather than wide-angle nozzles. The variation of the heat transfer coefficients of individual tubes across the bundle is generally smaller under such conditions, as to be shown by the data below.

The influence of saturation temperature on the tube bundle effect is demonstrated by comparing between Figs. 3 and 4, where data for standard-angle nozzles, 0.14 kg/s m spray flow rate and 5.08 cm nozzle height are presented. The only difference between the two figures is in the saturation temperature, −23.3°C for Fig. 3, as

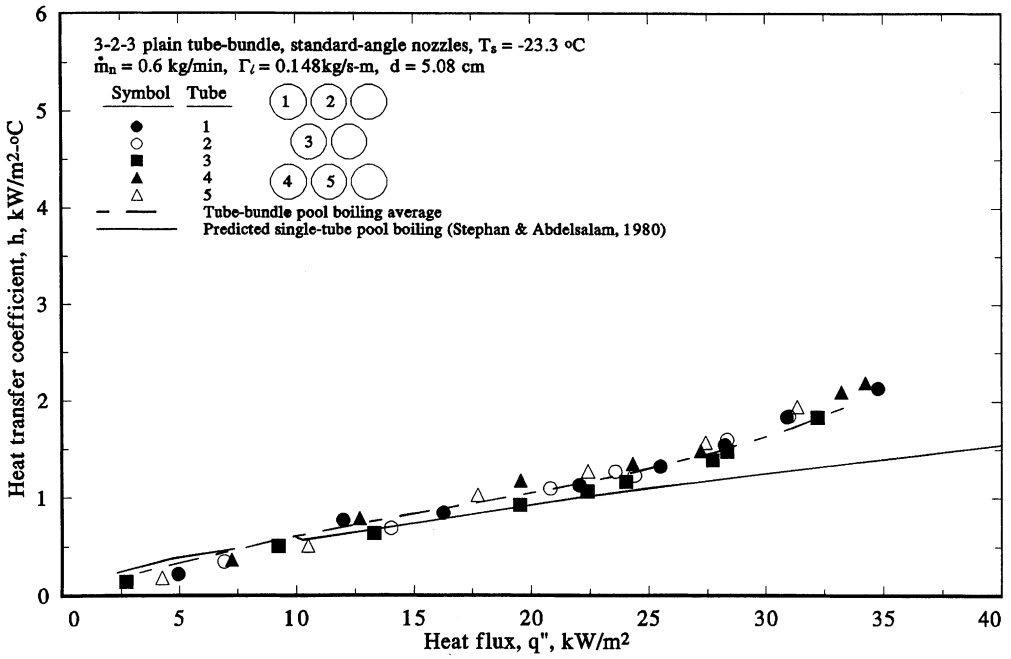

Fig. 3. Spray evaporation performance with standard-angle nozzles at −23.3°C, $d = 5.08$ cm, $\Gamma_l = 0.148$ kg/s m.

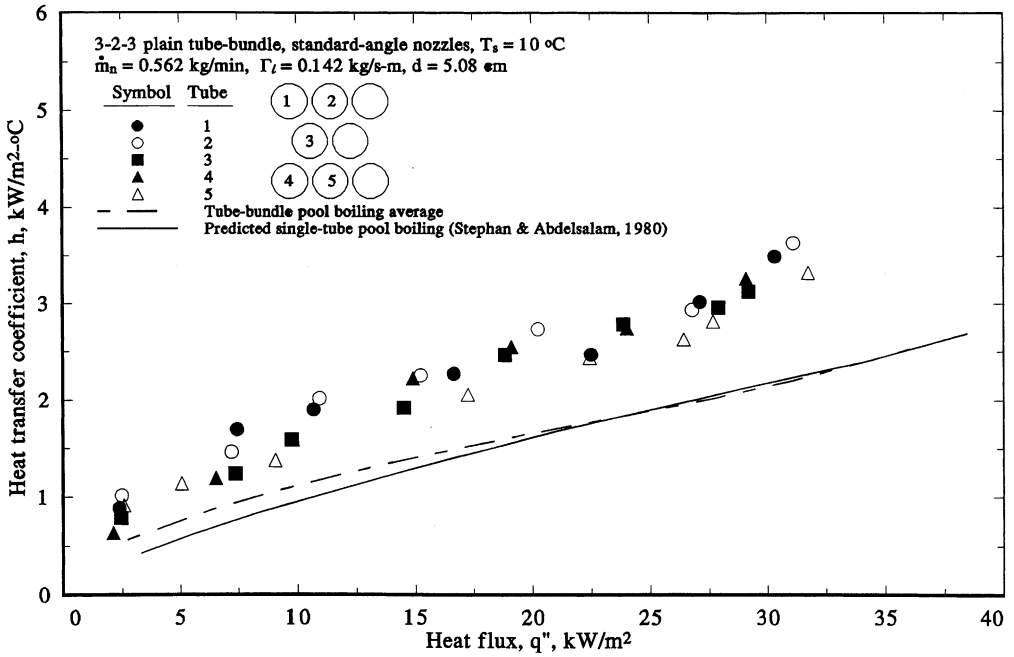

Fig. 4. Spray evaporation performance with standard-angle nozzles at 10°C, $d = 5.08$ cm, $\Gamma_l = 0.142$ kg/s m.

compared with that of 10°C for Fig. 4. The h data of individual tubes at −23.3°C (Fig. 3) scatter in a smaller range than that of 10°C in Fig. 4. Nucleate boiling is weak at a low saturation temperature because a greater wall superheat or heat flux is required to initiate nucleate boiling in a liquid film at a lower saturation temperature [31]. As a result, spray evaporation coefficient data at a low temperature are not markedly higher than pool boiling data of single tube [10,32]. Therefore, in Fig. 3, data of all tubes in the bundle are close to the pool boiling data with slightly higher spray evaporation coefficients in the top row due to the effect of liquid droplet impingement, and thus resulting in a small variation of individual tube coefficients across the bundle. Similar performance is shown by the square-pitch tube bundle data in Figs. 5 and 6. The h data of individual tubes at −23.3°C (Fig. 5) scatter in a smaller range than those at 10°C in Fig. 6.

The present data suggest that a lower spray flow rate may result in a weaker tube bundle effect. Comparison between Figs. 7 and 8 for −1.1°C with standard-angle nozzles and 5.08 cm nozzle height reveals that at a smaller spray flow rate, the variation of heat transfer coefficient among individual tubes across the bundle is smaller. For instance, at around 20 kW/m^2 heat flux, the variation in h at 0.144 kg/s m is approximately 15% (Fig. 7), while that at 0.724 kg/s m is about 35% (Fig. 8). The larger variation is mainly because of higher heat transfer coefficients in the top row due to a stronger liquid droplet impingement effect at a larger spray flow rate, while the bottom row coefficients basically remain unaffected by the change in spray flow rate. Similar result is demonstrated by comparing Figs. 4 and 9 at 10°C. The scatter range of individual tube coefficients increases as spray flow rate is increased from 0.142 to 0.706 kg/s m. The data of the 3×3 square-pitch tube bundle generally agree with the triangular-pitch bundle, but the change of coefficient scatter range with spray flow rate is not as significant.

On the other hand, under the same test condition as Figs. 7 and 8, if wide-angle nozzles instead of standard-angle nozzles are used, tube bundle effect does not depend on spray flow rate, a behavior considered to be related to the low-momentum liquid spray provided by the wide-angle nozzles. The small liquid droplets of low velocity generated by the wide-angle nozzles apparently did not create a significant difference in terms of liquid droplet impingement effect when spray flow rate was varied. In general, the present experimental results suggest that the dependence of tube bundle effect on spray flow rate is not significant at a low saturation temperature, a large nozzle height, and when wide-angle nozzles are employed. Similar result was also observed with square-pitch tube bundle. It is noteworthy that the present results are based on the data of a small bundle. Different performances may be observed with a large tube bundle particularly in the lower rows near the onset of dryout.

The significance of tube bundle effect may also depend on nozzle height. Data in both Figs. 4 and 10 were

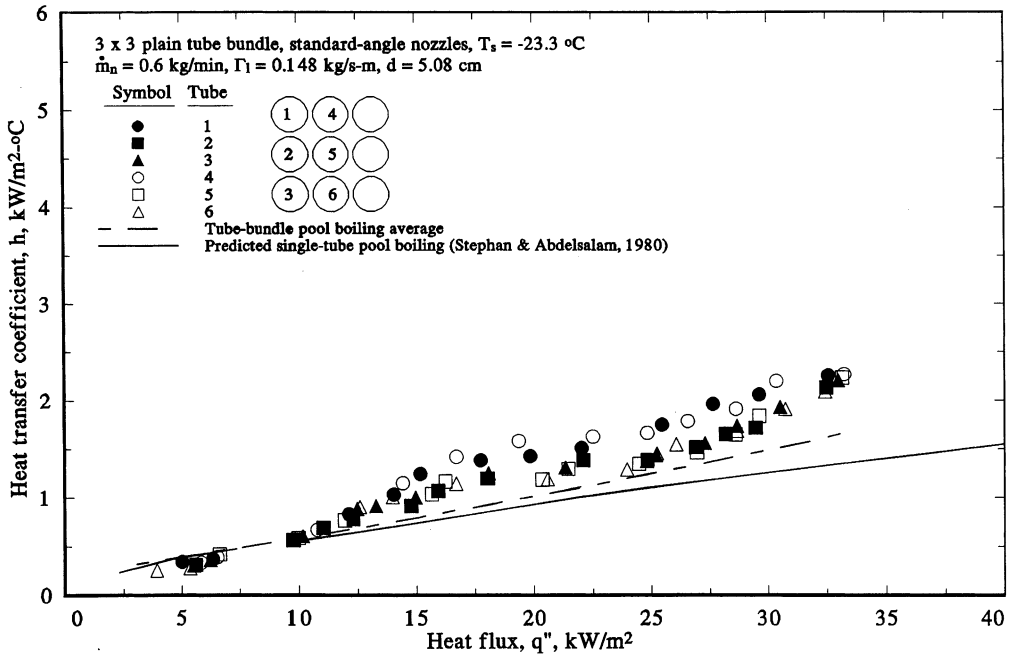

Fig. 5. Spray evaporation performance with standard-angle nozzles at −23.3°C, $\Gamma_l = 0.148$ kg/s m, $d = 5.08$ cm.

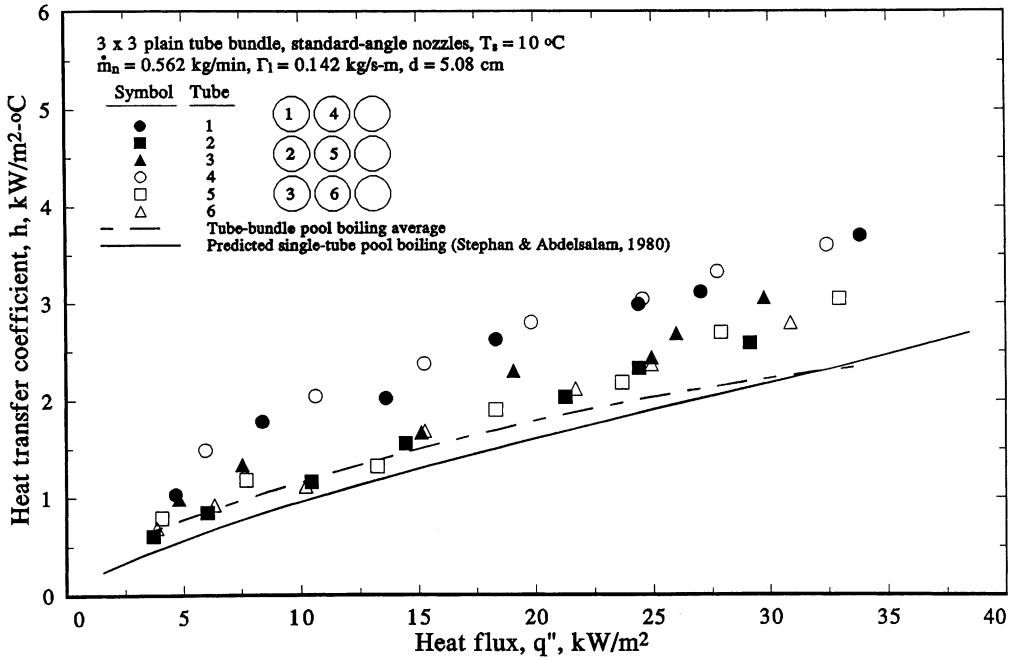

Fig. 6. Spray evaporation performance with standard-angle nozzles at 10°C, $\Gamma_l = 0.142$ kg/s m, $d = 5.08$ cm.

taken at 10°C, $\Gamma_l = 0.142$ kg/s m, and with standard-angle nozzles. Nozzle height d is the only difference in the test condition between the two figures that the nozzle height for Fig. 10 is twice as large as that for Fig. 4. A higher spray flow rate, $\dot{m}_n$, in Fig. 10 provides the same spray flow rate per unit tube length, Γ_l, as that in Fig. 4 with a smaller d. Data in these two figures suggest that a larger d results in a larger variation in h across the tube

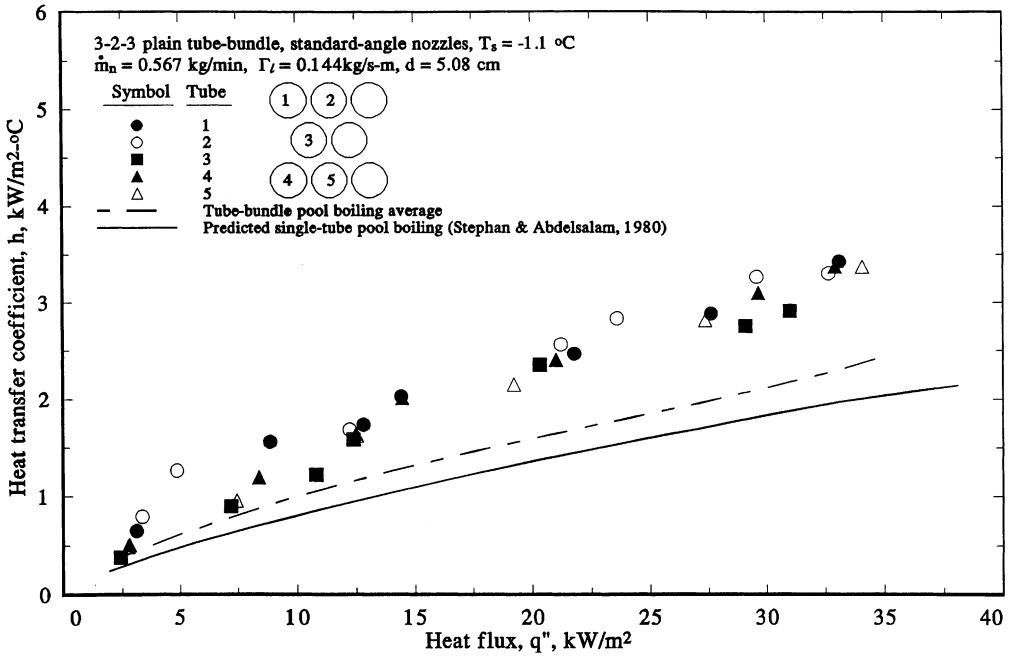

Fig. 7. Spray evaporation performance with standard-angle nozzles at −1.1°C, $d = 5.08$ cm, $\Gamma_l = 0.144$ kg/s m.

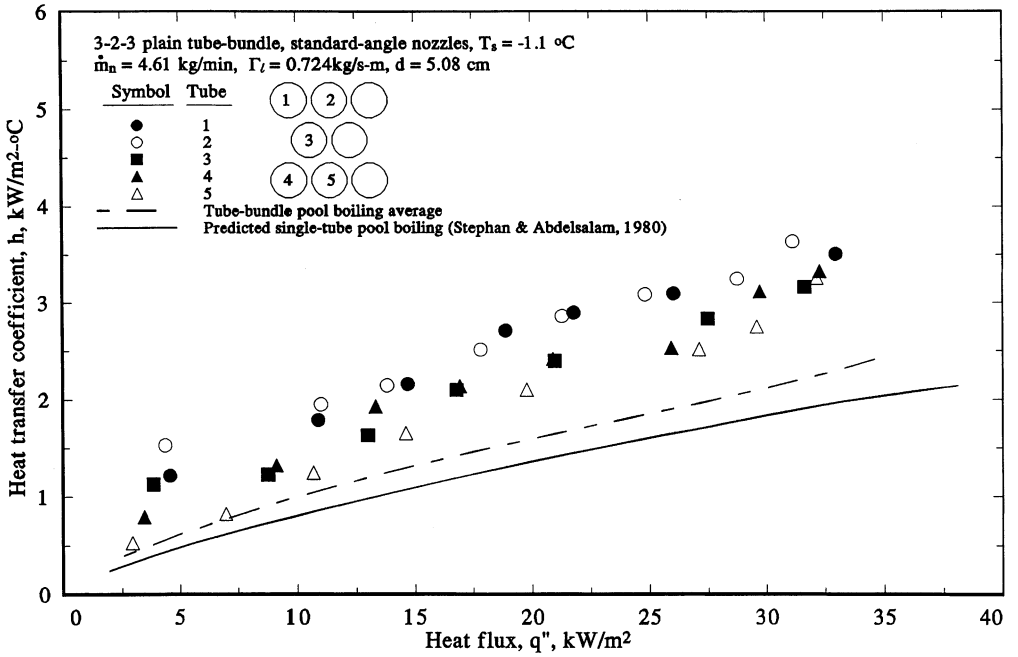

Fig. 8. Spray evaporation performance with standard-angle nozzles at −1.1°C, $d = 5.08$ cm, $\Gamma_l = 0.724$ kg/s m.

bundle, with the average bundle coefficient slightly decreasing with d. Comparing the individual tube data in two figures, the data of tubes in the top rows are close to each other. However, the data in the lower rows for $d = 10.2$ cm are lower than that for $d = 5.08$ cm. In other words, the larger variation in individual coefficients at a large d is mainly due to the lower coefficients of tubes in the lower rows. The low coefficients in the

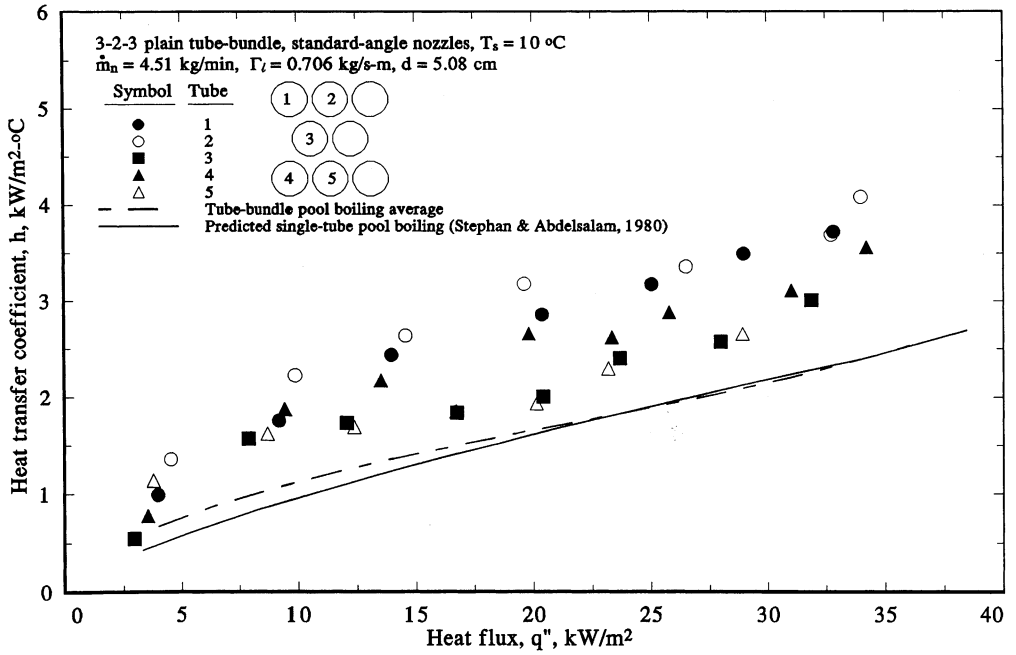

Fig. 9. Spray evaporation performance with standard-angle nozzles at 10°C, $d = 5.08$ cm, $\Gamma_l = 0.706$ kg/s m.

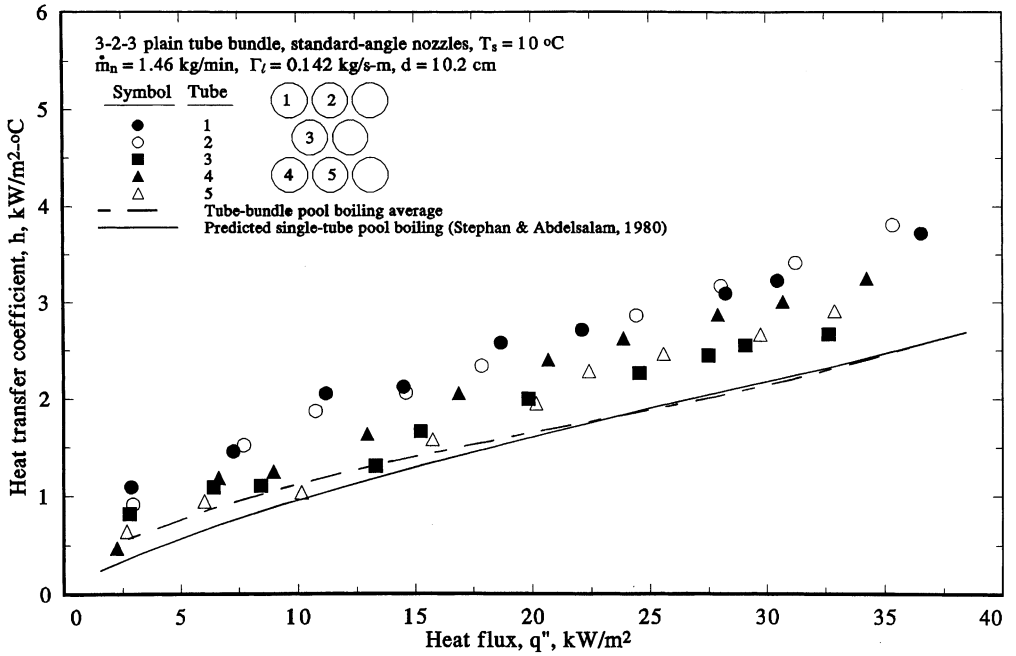

Fig. 10. Spray evaporation performance with standard-angle nozzles at 10°C, $d = 10.2$ cm, $\Gamma_l = 0.142$ kg/s m.

lower rows at a large d is considered to be due to the nonuniform axial spray flow rate distribution in the tube bundle. Following the analysis of Chyu et al. [27], the spray flow rate distribution from an array of spray nozzles is shown qualitatively in Fig. 11. Assuming uniform spray flow rate density distribution within an impact area, the spray flow rate is theoretically twice as large in the overlapped regions between two adjacent

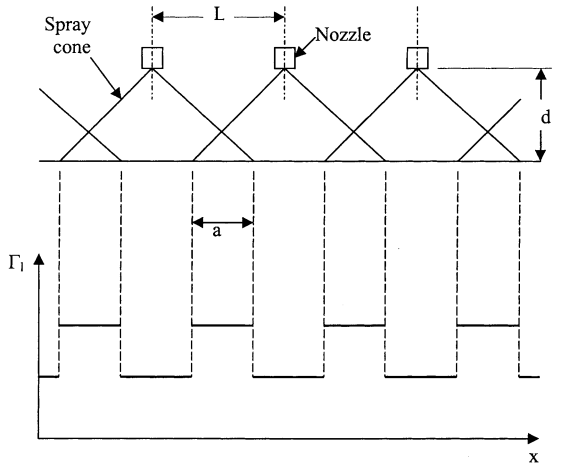

Fig. 11. Axial spray flow rate distribution under a nozzle array.

spray nozzles compared with the nonoverlapped regions directly below the nozzles. For a fixed L (spacing between two nozzles), the overlap length, a, increases with nozzle height, d. Therefore, the spray flow rate distribution in the axial direction is less uniform for a larger nozzle height. The nonuniformity of the axial spray flow distribution causes a decrease in the average heat transfer coefficient across the length of the tube. Such effect was apparently overshadowed by the effect of liquid droplet impingement on the top row. Hence, for a larger d, coefficients of tubes in the top row are close to that of a smaller d, but coefficients of tubes in the lower rows are lower than that of a smaller d, as shown in Figs. 4 and 10. The result is a larger variation in individual tube coefficients and a slight decrease in the average tube bundle coefficient. The present experimental result suggests that the effect of d on the variation of h is not significant at a low saturation temperature or when wide-angle nozzles are employed. The effect is also not significant with the square-pitch tube bundle.

The effect of nozzle type on the variation of individual tube coefficients across the bundle can be illustrated by comparing Figs. 4 and 12. Data in both figures were collected at 10°C, 0.142 kg/s m spray flow rate and 5.08 cm nozzle height. The only difference is that data in Fig. 4 were taken with standard-angle nozzles, while data in Fig. 12 were with wide-angle nozzles. The data show that wide-angle nozzles provide a larger variation of h than standard-angle nozzles. It was observed during the experiment that wide-angle nozzles generated liquid droplets smaller in size and moving at a lower velocity than standard-angle nozzles. The lower velocity of liquid droplet impingement on the top row provided a more favorable condition for nucleate boiling which was an important mode of heat transfer at this high saturation temperature (10°C). Therefore, higher coefficients were observed in the top row under wide-angle nozzles (Fig. 12) than that under standard-angle nozzles (Fig. 4). This was the primary mechanism causing a larger variation of individual tube coefficients across a bundle subjected to wide-angle spray nozzles. The influence of wide-angle

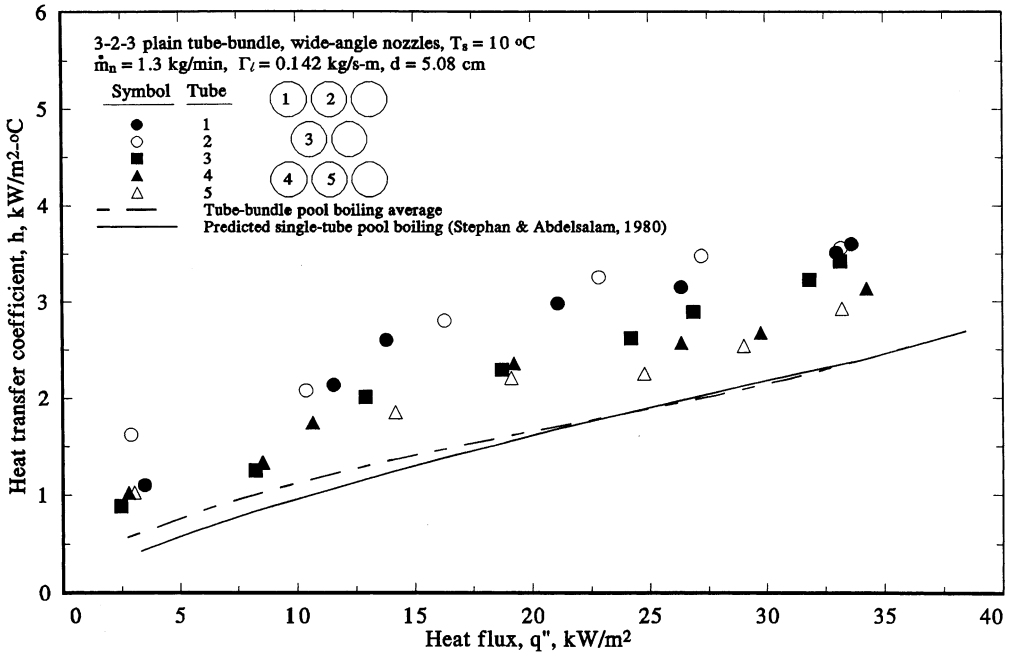

Fig. 12. Spray evaporation performance with wide-angle nozzles at 10°C, $d = 5.08$ cm, $\Gamma_l = 0.142$ kg/s m.

nozzles on tube bundle effect is also significant at −1.1°C, but is not significant at the low temperature of −23.3°C where nucleate boiling is weak. The effect is also not significant with square-pitch tube bundle.

Comparison between Figs. 4 and 6 shows that square-pitch bundle pattern results in a larger tube bundle effect than triangular-pitch bundle. Data in both Figs. 4 and 6 are for 10°C, 0.142 kg/s m spray flow rate, 5.08 cm nozzle height, and with standard-angle nozzles, while Fig. 4 is for triangular-pitch tube bundle, and Fig. 6 is for square-pitch tube bundle. The h data in Fig. 6 scatter in a wider range than those in Fig. 4. There is not much difference in the data in the top row. The larger scatter range with the square-pitch tube bundle is mainly due to lower heat transfer coefficients of tubes in the lower rows. At the present test saturation temperature of 10°C, nucleate boiling prevails, and two-phase flow convection becomes an important mode of heat transfer within the bundle. The two-phase flow pattern within a tube bundle in spray evaporation is similar to that within a tube bundle in pool boiling except that the flow direction is reversed. In pool boiling, the direction of two-phase flow is upward due to buoyancy, while the flow direction is downward in spray evaporation due to gravity. In both cases, two-phase flow convection provides increased turbulence induced by bubbles impinging onto and sliding over the tube walls, as well as thin film evaporation on tube walls as bubbles slide across. For the same pitch ratio and tube diameter, it is a geometrical fact that the space between tubes in a triangular-pitch bundle is narrower than that in a square-pitch bundle. The narrower flow passages make it more likely for bubbles to be in contact with tube walls, therefore achieving higher heat transfer coefficients in a triangular-pitch bundle. Also, the zigzag passages between tubes in a triangular-pitch bundle increase the chance for bubbles to impinge and to slide over tube walls. The distance that a bubble has to travel across a triangular-pitch bundle is longer than that of a square-pitch bundle. The more contact between tubes and flowing bubbles, the higher the average heat transfer coefficient. Therefore, the heat transfer coefficients of tubes in a triangular-pitch bundle, particularly in lower rows, are higher than those of a square-pitch bundle at a high saturation temperature when nucleate boiling prevails. The smaller scatter range of heat transfer coefficient in Fig. 4 is due to the higher coefficients in the lower rows than those in Fig. 6.

4. Conclusions

The present data suggest that in spray evaporation of ammonia using spray nozzles, tube bundle effect is less significant at a lower saturation temperature, a lower spray flow rate, a smaller nozzle height, or with standard-angle rather than wide-angle nozzles. The data also suggest that square-pitch bundle pattern demonstrates a larger tube bundle effect than triangular-pitch pattern. The mechanism causing variation of individual tube heat transfer performance within the bundle was investigated.

Acknowledgements

Support for this project was provided by the American Society of Heating, Refrigerating, and Air-Conditioning Engineers (ASHRAE RP-725). The guidance from the monitoring Technical Committee 1.3 is greatly appreciated.

References

[1] W.F. Stoecker, Growing opportunities for ammonia, in: Proceedings of the International Institute of Ammonia Refrigerant, Annual Meeting, Austin, 1989.
[2] Z.H. Ayub, S.K. Knewitz, Limited inventory ammonia falling film spray evaporator, in: Proceedings of the International Institute of Ammonia Refrigerant, Annual Meeting, 1991, pp. 61–78.
[3] S.A. Moeykens, M.B. Pate, Spray evaporation heat transfer of R-134a on plain tubes, ASHRAE Trans. 100 (2) (1994) 173–184.
[4] S.A. Moeykens, M.B. Pate, The effects of nozzle height and orifice size on spray evaporation heat transfer performance for a low-finned triangular-pitch tube bundle with R134a, ASHRAE Trans. 101 (2) (1995) 420–433.
[5] S.A. Moeykens, J.E. Kelly, M.B. Pate, Spray evaporation heat transfer performance of R-123 in tube bundles, ASHRAE Trans. 102 (2) (1996) 259–272.
[6] S.A. Moeykens, W.W. Huebsch, M.B. Pate, Heat transfer of R-134a in single-tube spray evaporation including lubricant effects and enhanced surface results, ASHRAE Trans. 101 (1) (1995) 111–123.
[7] S.A. Moeykens, B.J. Newton, M.B. Pate, Effects of surface enhancement, film-feed supply rate, and bundle geometry on spray evaporation heat transfer performance, ASHRAE Trans. 101 (2) (1995) 408–419.
[8] S.A. Moeykens, M.B. Pate, Effect of lubricant on spray evaporation heat transfer performance of R-134a and R-22 in tube bundles, ASHRAE Trans. 102 (1) (1996) 410–426.
[9] J.R. Thome, Falling film evaporation: state-of-the-art review of recent work, Enhanced Heat Transfer 6 (1999) 263–277.
[10] X. Zeng, M.-C. Chyu, Z.H. Ayub, Evaporation heat transfer performance of nozzle-sprayed ammonia on a horizontal tube, ASHRAE Trans. 101 (1) (1995) 136–149.
[11] X. Zeng, M.-C. Chyu, Z.H. Ayub, Performance of nozzle-sprayed ammonia evaporator with square-pitch plain-tube bundle, ASHRAE Trans. 103 (2) (1997) 68–81.
[12] R.B. Cox, Some factors affecting heat transfer coefficients in the horizontal tube multiple effect (HTME) desalination process, in: Proceedings of the Third International

Symposium on Fresh Water from the Sea, vol. 1, 1970, pp. 247–263.
[13] W.J. Prince, Enhanced tubes for horizontal evaporator desalination process, M.S. Thesis, University of California, Los Angeles, 1971.
[14] C.J. Cannizaro, J.Z. Karpf, N. Kosowski, A.S. Pascale, Fourth report on horizontal-tube multiple-effect (HTME) process pilot plant test program, INT-OSW-RDPR-74-967, US Department of the Interior, 1972.
[15] J.Z. Karpf, R.S. Pascale, Fifth report on horizontal-tube multiple-effect (HTME) process pilot plant test program. INT-OSW-RDPR-74-963, US Department of the Interior, 1972.
[16] I.H. Newson, Heat transfer characteristics of horizontal tube multiple effect evaporators, Final Report INCRA Project No. 267, Chemical Engineering Division, Atomic Energy Research Establishment, Harwell, England, 1976.
[17] L. Hillis, J.J. Lorenz, D.T. Yung, N.F. Sather, OTEC Performance test of the union carbide sprayed bundle evaporator, Department of Energy Report ANL OTEC-PS-3, 1979.
[18] H.D. Fricke, A.M. Czikk, Enhanced OTEC sprayed bundle evaporator performance studies, Adv. Enhanced Heat Transfer ASME HTD (1979) 23–29.
[19] A.M. Czikk, H.D. Fricke, E.N. Ganic, B.I. Sharma, Fluid dynamics and heat transfer studies of OTEC heat exchangers. in: Proceedings of the Fifth Ocean Thermal Energy Conversion Conference, 1978, pp. VI-181–236.
[20] J.J. Lorenz, D. Yung, P.A. Howard, C.B. Panchal, F.W. Poucher, OTEC-1 power system test program: performance of one-megawatt heat exchangers, Department of Energy Report ANL/OTEC-PS-10, 1981.
[21] G.N. Danilova, V.G. Burkin, V.A. Dyundin, Heat transfer in spray-type refrigerator evaporators, Heat Transfer – Sov. Res. 8 (6) (1976) 105–113.
[22] C.M. Sabin, H.F. Poppendiek, Film evaporation of ammonia over horizontal round tubes, in: Proceedings of the Fifth OTEC Conference, Miami Beach, FL, 1978, pp. VI-237–260.
[23] X. Zeng, M.-C. Chyu, Z.H. Ayub, Ammonia spray evaporation heat transfer performance of single low-fin and corrugated tubes, ASHRAE Trans. 104 (1) (1998) 185–196.
[24] J.E. Snyder, A.M. Sprouse, Design of 1MWe ocean thermal energy conversion (OTEC) heat exchangers for ocean testing, Heat transfer in ocean thermal energy conversion (OTEC) systems, ASME HTD 12 (1980) 17–26.
[25] G. Kocamustafaogullari, I.Y. Chen, Horizontal tube evaporators, Part I. Theoretically-based correlations, Int. Commun. Heat Mass Transfer 16 (1989) 487–499.
[26] X. Zeng, M.-C. Chyu, Z.H. Ayub, Characteristic study of sprayed fluid flow in a tube bundle, ASHRAE Trans. 100 (1) (1994) 63–72.
[27] M.-C. Chyu, X. Zeng, Z.H. Ayub, Nozzle-sprayed flow rate distribution on a horizontal tube bundle, ASHRAE Trans. 101 (2) 1995.
[28] R.H. Perry, C.H. Chilton, Chemical Engineers' Handbook, sixth ed., McGraw-Hill, New York, 1984.
[29] W.M. Rohsenow, J.P. Hartnett, E.N. Ganic, Handbook of Heat Transfer Applications, second ed., McGraw-Hill, New York, 1985 (Chapter 4).
[30] V. Gnielinski, New equations for heat and mass transfer in turbulent pipe and channel flow, Int. Chem. Eng. 16 (1976) 359–368.
[31] K.R. Chun, R.A. Seban, Heat transfer to evaporating liquid films, J. Heat Transfer (1971) 391–396.
[32] K. Stephan, M. Abdelsalam, Heat-transfer correlations for natural convection boiling, Int. J. Heat Mass Transfer 23 (1980) 73–87.